Novel Corner Detection Methods Leveraging Gradient Isotropy and Structure Tensor Analysis

Mustafa Sadeghi[1], **Mohamad Mehdi Khorsand Aalam**[1], and **Hadi Sadoghi Yazdi**[*1,2]

[1]Department of Computer Engineering, Ferdowsi University of Mashhad, Mashhad, Iran
[2]Center of Excellence in Soft Computing and Intelligent Information Processing, Ferdowsi University of Mashhad, Mashhad, Iran

Abstract

we introduce three novel corner detection algorithms that leverage the concept of *gradient isotropy* within the framework of the *structure tensor matrix* to enhance detection accuracy and robustness. By analyzing the eigenvalues of the structure tensor, we assess the isotropy of image gradients, distinguishing corners from edges and flat regions. The proposed corner response functions—Q_{EG}, Q_s, and Q_H—utilize different mathematical formulations to measure gradient isotropy. The Q_{EG} method computes the ratio of the determinant to the trace of the structure tensor, emphasizing regions with high gradient isotropy. The Q_s method analyzes the squared structure tensor matrix to capture higher-order gradient interactions, enhancing sensitivity to subtle isotropic variations. The Q_H method incorporates the Heinz mean with a tunable parameter, providing flexibility in measuring gradient isotropy to balance sensitivity and robustness. We evaluate the performance of our algorithms through extensive experiments on both synthetic and real-world images, including challenging conditions with noise and geometric transformations. The proposed algorithms exhibit robustness to rotation and shear transformations, accurately detecting corners even in complex textured images. Specifically, Q_H with geometric mean algorithm shows remarkable resilience in noisy environments. By integrating gradient isotropy analysis within the structure tensor framework, our methods provide reliable and adaptable tools for accurately identifying corners in diverse imaging conditions, thereby enhancing the performance of computer vision systems.

Keywords: Corner detection · Gradient isotropy · Structure tensor · High-order gradient analysis · Image processing ·

1 Introduction

Corner detection is a fundamental task in computer vision, playing a crucial role in applications such as feature extraction, image matching, object recognition, and motion tracking. Corners, often referred to as interest points or keypoints, are locations in an image where the intensity gradient exhibits significant variations in multiple directions. Accurate detection of these points is vital for the reliability and performance of numerous computer vision algorithms. A key concept in understanding and improving corner detection is the analysis of gradient isotropy and anisotropy. Isotropy refers to properties that are identical in all directions, whereas anisotropy refers to directional dependence. In the context of image gradients, isotropy implies that the gradient magnitudes are similar in all directions around a point, which is characteristic of corners. Anisotropy, on the other hand, indicates that the gradient has a dominant direction, typical of edges. The structure tensor matrix is a powerful mathematical tool used to capture the local gradient distribution in an image. it provides insight into the orientation and magnitude of intensity variations. The eigenvalues of the structure tensor represent the principal gradients in the local neighborhood. When both eigenvalues are large and approximately equal ($\lambda_1 \approx \lambda_2 \gg 0$), the region is isotropic, indicating a corner. When one eigenvalue is significantly

*Corresponding author: h-sadoghi@um.ac.ir

larger than the other ($\lambda_1 \gg \lambda_2$ or $\lambda_2 \gg \lambda_1$), the region is anisotropic, indicating an edge. When both eigenvalues are small and approximately equal ($\lambda_1 \approx \lambda_2 \approx 0$), the region is isotropic and flat.

By analyzing the isotropy of the gradient through the structure tensor, we can more effectively distinguish corners from edges and flat regions. This approach enhances the robustness of corner detection algorithms, particularly in challenging imaging conditions. In this paper, we propose three novel corner detection methods based on gradient isotropy. The first method, Q_{EG}, utilizes the eigenvalues of the structure tensor to measure the isotropy of gradient energy. By computing a corner response function based on the ratio of the determinant and the trace of the structure tensor, it emphasizes regions where the gradients are similar in all directions. The second method, Q_s, leverages higher-order gradient interactions by analyzing the squared structure tensor matrix. It amplifies subtle isotropic variations in the gradient field, enhancing sensitivity to corners in complex textures and noisy environments. The third method, Q_H, incorporates the Heinz mean and introduces a tunable parameter to flexibly measure gradient isotropy, providing an adjustable balance between sensitivity and robustness to adapt to specific application requirements.

By integrating Gaussian smoothing, adaptive thresholding, and non-maximum suppression, our approaches achieve high accuracy and robustness in corner detection across various imaging conditions. The main contributions of this paper are the introduction of three novel corner detection algorithms that utilize gradient isotropy for improved performance, providing a comprehensive analysis of isotropy and anisotropy in the context of the structure tensor and corner detection, and demonstrating the effectiveness of the proposed methods through extensive experiments on synthetic and real-world images, including evaluations under noise and geometric transformations.

1.1 Motivation

The motivation behind this work is to introduce three new methods for corner detection that focus on the utilization of gradient isotropy. we propose methods that enhance corner detection by incorporating the directional changes of image gradients. By emphasizing gradient isotropy, we aim to distinguish corners from other image features, such as edges and flat regions, more effectively. The three methods we propose explore different mathematical formulations and techniques, leveraging the structure tensor and higher-order gradient information to improve corner detection accuracy. These methods are designed to accurately detect corners even in challenging images, such as those with complex textures and geometric distortions, making them more reliable for a wide range of computer vision applications.

While our current work focuses on gradient-based methods, we recognize that integrating these techniques with deep learning could further enhance corner detection. After extracting corner-related features using mathematical operators, these features could potentially be used as inputs to deep neural networks. This approach may allow networks to gain a deeper understanding of complex image structures and corner features, even in the presence of noise or geometric transformations. Although we did not explore this integration in the present paper, it represents a promising direction for future research. The combination of traditional gradient-based methods and deep learning could significantly improve the accuracy and robustness of corner detection, making it adaptable to a wider range of real-world scenarios.

1.2 Paper Organization

The paper is organized as follows: In Section [2], we review the related work in the field of corner detection, with a focus on both mathematical operators and machine learning approaches. Section [3] introduces the corner response function as the proposed method for corner detection, which utilizes the concept of gradient isotropy. In Section [4], we present the algorithms for implementing these methods and detail the steps involved in their computation. Section [5] presents the experimental results, where we evaluate our methods in terms of corner localization accuracy, robustness to noise, and resistance to geometric transformations. We also discuss the performance of the proposed methods in comparison to Harris corner detection algorithm. Finally, Section [6] concludes the paper and outlines potential directions for future work in the area of corner detection.

2 Related Work

Corner detection has seen significant advancements across different domains, from mathematical operators to machine learning techniques, each offering unique contributions relevant to the objectives of this paper. The Förstner-Gülch operator, for instance, has proven effective for corner detection in noisy and geometrically distorted images, which is crucial for enhancing the reliability of feature extraction in real-world applications. This work aligns with our goal of improving robustness and precision in corner detection, particularly by focusing on advanced gradient techniques. Similarly, the fractional gradient operator proposed by Pan et al. introduces higher-order differentiation, an approach that inspires our exploration of gradient isotropy within the structure tensor framework, aiming to refine corner localization under challenging conditions. In the domain of machine learning, methods like the use of multi-layer perceptrons in event-based vision [13] highlight the growing role of learning-based approaches for extracting image gradients in asynchronous settings. These techniques provide insight into how machine learning can enhance corner detection in dynamic and sparse data environments, which is particularly relevant to our objective of developing adaptable algorithms for a variety of imaging scenarios. Furthermore, application-specific advancements, such as brain tissue segmentation in infant MRI images [7] and hardware-optimized methods for real-time corner detection [2], demonstrate the practical utility of corner detection in medical and embedded systems. These works are closely related to our approach, as they emphasize corner detection's importance in diverse fields and highlight the need for precision and robustness, motivating the introduction of our gradient-based techniques for improved performance across different imaging conditions.

2.1 Presentation of Mathematical Operators in Articles

The Förstner-Gülch operator [5]efficiently detects points, corners, and circular centers with robustness to noise, geometric distortions, and radiometric changes, making it versatile for various applications. Its advantages include distinctness in feature selection, invariance to transformations, and adaptability to different hardware platforms. However, the reliance on analyzing two image patches for corner detection introduces computational complexity. Mathematically, it utilizes least-squares matching to minimize discrepancies, leveraging gradient-based weighting to ensure precise localization and optimize feature stability across varying conditions. This work [10] proposes a robust and order-steerable image corner detector using a fractional gradient operator, which combines fractional-order forward and backward differentiation and integration. The new method, capable of achieving a 90° phase shift, offers an innovative approach to image gradient calculation. Experiments on simulated and real medical slices demonstrate that the proposed detector outperforms traditional corner detection methods, such as Harris and Shi–Tomasi, in terms of corner localization and noise robustness. This work proposes a new gradient that can be used for a wide range of corner detection operators.

This article [8] improves the corner detection method introduced by Mehrotra and Nichani by replacing isotropic Gaussian kernels with anisotropic Gaussian kernels[9]. This modification facilitates the detection of corners with acute angles, which was a limitation of the original method that only performed well with open angles. Experimental results demonstrate that the new method is significantly more robust and accurate, particularly in the presence of noise, and it can better identify half-edges. Additionally, this refined method outperforms other established corner detection techniques across various noise levels and image types. The authors conclude that due to its straightforward implementation and effectiveness, this method has the potential to become a valuable resource for the computer vision community.

This work [4] introduces a correlation-guided attention mechanism for enhanced corner detection in visual tracking. Utilizing a Siamese network and dual-stage attention modules, it achieves precise corner localization by combining pixel-wise and channel-wise attention, making it robust against background distractors. The Fully-Convolutional Siamese Network (Bertinetto et al., 2016) [3] serves as a foundation for efficient object tracking, leveraging end-to-end learned similarity metrics. Its cross-correlation operation underpins the attention mechanisms in recent frameworks like Correlation-Guided Attention (2024). By extending the Siamese network's similarity computation to spatial attention weighting, these methods significantly improve corner localization precision, demonstrating the effectiveness of combining Siamese architectures with attention techniques.

2.2 Analysis of Articles from a Machine Learning Perspective

The work [13]tackle corner detection in event-based vision . They introduce multi-layer perceptron to identify corners. Several researchers have developed methods to extract image gradients directly from event streams, providing a foundation for gradient-based corner detection in event-based vision. Gradient-based approaches like these show promise for event cameras but must account for the asynchronous, sparse nature of event data to be effective. The paper [14]presents an innovative end-to-end method for sub-pixel checkerboard corner localization, critical for high-precision vision measurement tasks. Their approach, combines offset prediction and continuous heat-map matching to achieve state-of-the-art accuracy on both synthetic and real-world datasets. This method demonstrates superior robustness, making it ideal for challenging scenarios in vision measurement applications. While this approach achieves high accuracy and robustness, its limitations include high computational complexity, reliance on extensive training data, reduced interpretability, and potential overfitting to synthetic datasets. These challenges make it less suitable for resource-constrained or real-time applications, highlighting the need for efficient mathematical approaches. The mathematical methods categorized in [1] are divided into direct and indirect approaches. Direct methods, such as cosine-based detection, and the triangle principle, are computationally simpler but often sensitive to noise. In contrast, indirect methods, including Curvature Scale Space and Contour Difference, offer better robustness at the cost of higher computational complexity. These distinctions emphasize the trade-offs involved in selecting suitable methods for specific image processing tasks.

2.3 Evaluation of Corner Detection Applications in Articles

The article [7]proposed a four-phase automated system for brain tissue segmentation and classification in infant MRI images. They utilized Forstner Corner Detection to identify seed points for the Seeded Region Growing segmentation process, coupled with sparse autoencoders for classification. Their method achieved a high Dice Similarity Coefficient, outperforming state-of-the-art techniques and addressing challenges posed by low-contrast infant brain MRIs. In [2]present a novel ultra-efficient carbon nanotube field-effect transistor-based corner detection hardware designed for real-time image processing, addressing limitations of traditional algorithms like HARRIS and SIFT due to their computational complexity. Their method uses a lightweight algorithm optimized for circuit-level implementation with high noise immunity, achieving significant gains in speed, energy efficiency, and robustness over existing solutions. The process involves comparing pixel intensities to a threshold (T = 15) using an 8-bit full-subtractor and a streamlined comparator circuit. The subtraction logic ensures absolute differences are efficiently calculated, minimizing hardware overhead while maintaining accuracy in corner detection.

An intensity-based corner detector leveraging a novel corner response function is introduced in [12]. The method evaluates intensity differences within a 3x3 pixel neighborhood to generate a highly effective corner response map. Compared to seven well-established detectors, it demonstrates superior accuracy in corner localization, significantly reducing missed corners and false positives in benchmark tests. The results highlight the robustness and precision of the proposed approach, making it a reliable tool for tasks requiring precise corner detection.

Another study [11] proposes two innovative techniques—laser triangulation and hybrid Harris corner detection—for analyzing the pressure-volume diagram of a flat alpha-type Stirling engine. The hybrid Harris corner detection method shows superior accuracy in determining key engine parameters such as speed, phase angle, and indicated power, outperforming existing techniques. Detailed descriptions of the experimental setup, data acquisition processes, and mathematical models are provided, demonstrating the reliability and effectiveness of these methods. The findings contribute to improved approaches for evaluating Stirling engine performance and validating theoretical models, with both methods offering practical accuracy for real-world applications.

3 The proposed methods

In this section we introduces three corner response functions, $\boldsymbol{Q_{EG}}$[3.2], $\boldsymbol{Q_s}$[3.3], and $\boldsymbol{Q_H}$[3.4], each designed to focus on the energy of gradients in the x, y, xy, and yx directions. These operators are specifically formulated to effectively capture and analyze gradient energy patterns, addressing the unique requirements of corner detection by leveraging the concept of gradient isotropy. The detailed formulation and characteristics of these operators are presented in the following subsections.

The Structure Tensor Matrix [3.1] is indispensable for corner detection as it provides a unified framework for capturing local gradient information and gradient isotropy analysis. By representing intensity variations within a neighborhood, it enables precise analysis of the strength and orientation of local features. This capability is critical for distinguishing corners from edges and flat regions, as corners typically exhibit significant variations in gradient magnitude and direction. The structure tensor matrix ensures a robust mathematical foundation for these methods,making it a cornerstone of effective corner detection techniques.

3.1 Structure Tensor Matrix

In this section, the construction of the **structure tensor matrix** is presented, serving as the foundational element of the proposed corner detection method. The structure tensor encapsulates the local gradient information of an image, providing a robust representation of intensity variations within a neighborhood surrounding each pixel. Let $I(x, y)$ denote a discrete gray-scale image defined over a spatial domain, it is assumed that the integration area Γ is sufficiently small such that smoothing this area with a Gaussian filter $g(x, y, \sigma)$ effectively reduces noise in the image. Consequently, none of the correlation integrals below can be treated as converged statistical quantities. It is also assumed that the image is continuously differentiable everywhere.

$$s(x, y, \sigma) = I(x, y) * g(x, y, \sigma) = \iint_{\Gamma} I(u, v) \frac{1}{\sqrt{2\pi\sigma^2}} e^{-\frac{(x-u)^2+(y-v)^2}{2\sigma^2}} \, du \, dv$$

Also in the image region with $\Omega \subset \mathbb{Z}^2$.

$$s(i, j; \sigma) = (I * g)(i, j; \sigma) = \sum_{m=-M}^{M} \sum_{n=-N}^{N} I(i - m, j - n) \, g(m, n; \sigma),$$

where the discrete Gaussian kernel $g(m, n; \sigma)$ is defined as: $g(m, n; \sigma) = \frac{1}{2\pi\sigma^2} \exp\left(-\frac{m^2+n^2}{2\sigma^2}\right)$. The parameters M and N define the size of the kernel, typically chosen to cover the significant values of the Gaussian function. The parameter σ determines the standard deviation of the Gaussian kernel, with larger values leading to greater smoothing and noise attenuation at the expense of potential loss of fine image details. The choice of σ must balance noise reduction and feature preservation, typically selected based on the specific requirements of the application. Subsequently, the image gradients are computed by differentiating the smoothed image $s(i, j; \sigma)$ with respect to the spatial coordinates.

$$f_x(i, j) = \left.\frac{\partial s}{\partial x}\right|_{(i,j)}, \quad f_y(i, j) = \left.\frac{\partial s}{\partial y}\right|_{(i,j)}.$$

Figure 1: Demonstration of the effect of Gaussian filtering with varying standard deviations (σ) on a chessboard image. The original image (a) exhibits sharp edges and clear features. The addition of noise (b) introduces high-frequency variations, degrading the image quality. Gaussian filters with increasing standard deviations ($\sigma = 1, 2, 3$) progressively smooth the image, effectively suppressing noise but also causing a reduction in edge sharpness and fine detail preservation. This trade-off highlights the importance of selecting an appropriate σ value to balance noise reduction and feature retention in image preprocessing.

These partial derivatives represent the rate of change of intensity along the x- and y-axes, respectively, and capture the local directional variations within the image. Let us consider cross correlations between f_x and f_y as :

$$\mathbf{S} = \left\langle \begin{bmatrix} f_x \\ f_y \end{bmatrix} \begin{bmatrix} f_x & f_y \end{bmatrix} \right\rangle = \begin{bmatrix} \langle f_x^2 \rangle & \langle f_x f_y \rangle \\ \langle f_y f_x \rangle & \langle f_y^2 \rangle \end{bmatrix} = \begin{bmatrix} S_{xx} & S_{xy} \\ S_{yx} & S_{yy} \end{bmatrix}$$

where, $\langle \cdot \rangle = \iint_\Gamma \cdot \, dx \, dy$, an integral is taken over the small region Γ. In the image $\langle \cdot \rangle$ denotes an averaging operation over a local neighborhood $\Gamma \subset \Omega$ centered at (i, j). Specifically, the averaging is defined as:

$$\langle h \rangle = \sum_{k=-w}^{w} \sum_{l=-w}^{w} h(i+k, j+l)\, w(k, l),$$

with $w(k, l)$ being a weighting function that assigns importance to the contributions from different locations within the neighborhood, often chosen as a Gaussian window to emphasize pixels near the center. The window radius w determines the size of the neighborhood Γ, resulting in a window of size $(2w + 1) \times (2w + 1)$. The components of the structure tensor $\mathbf{S}$ are explicitly given by:

$$S_{mn} = \langle f_m f_n \rangle = \sum_{k=-w}^{w} \sum_{l=-w}^{w} f_m(i+k, j+l) f_n(i+k, j+l)\, w(k, l),$$

where $m, n \in \{x, y\}$. Given that $S_{xy} = S_{yx}$ due to the commutative property of multiplication, the structure tensor $\mathbf{S}$ is a symmetric, positive semi-definite 2×2 matrix. S_{xx} quantifies the variance of the gradient along the x-direction within the neighborhood Γ, reflecting horizontal intensity variations. S_{yy} quantifies the variance along the y-direction, capturing vertical intensity variations. S_{xy} measures the covariance between the x- and y-directional gradients, providing insight into the correlation and orientation of local intensity changes.

The images in Figure (2) effectively illustrate the components of the structure tensor matrix and their role in analyzing image gradients. The original chessboard image (1) provides a high-contrast and structured pattern, ideal for testing the performance of gradient-based analysis methods. The heatmap of S_{xx} (2a) highlights horizontal gradient magnitudes, with bright vertical bands indicating significant intensity changes along the horizontal direction. These correspond to the vertical edges of the chessboard squares, showcasing S_{xx}'s sensitivity to horizontal gradient variations. The heatmap of S_{yy} (2b) emphasizes vertical gradient magnitudes, with bright horizontal bands representing intensity changes along the vertical direction. This captures the horizontal edges of the chessboard squares, demonstrating S_{yy}'s ability to detect vertical gradients. The S_{xy} heatmap (2c) visualizes the correlation between horizontal and vertical gradients. Higher values, shown as bright spots, appear at corners where intensity changes occur in both directions, making S_{xy} particularly useful for corner detection. This component complements S_{xx} and S_{yy} by providing additional information about areas of combined gradient variations. These visualizations collectively demonstrate how the structure tensor matrix components work together to analyze and differentiate between edges, flat regions, and corners in the image.

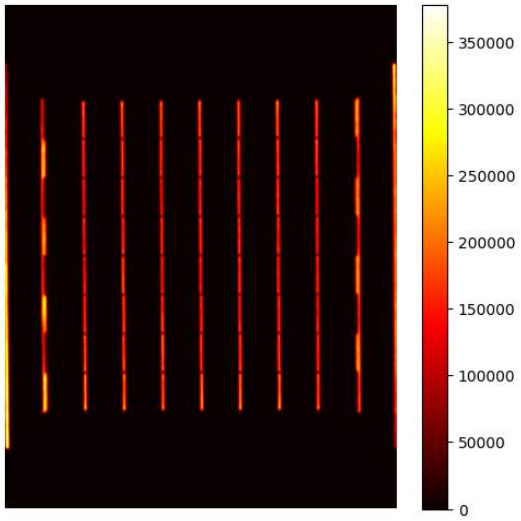

(a) The heatmap of S_{xx} illustrates the horizontal gradient magnitude, emphasizing vertical edges in the chessboard pattern. High-intensity responses (bright areas) occur where significant intensity changes are present along the horizontal direction, corresponding to the vertical boundaries of the chessboard squares.

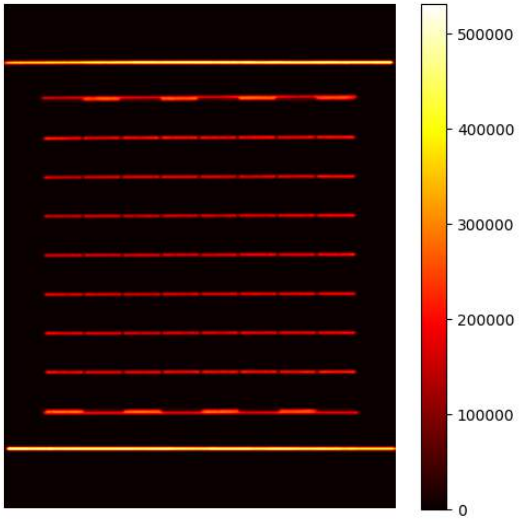

(b) The heatmap of S_{yy} visualizes the vertical gradient magnitude, highlighting horizontal edges in the chessboard pattern. Bright regions indicate strong vertical intensity variations, particularly along the horizontal boundaries of the squares, aligning with the structural transitions in the pattern.

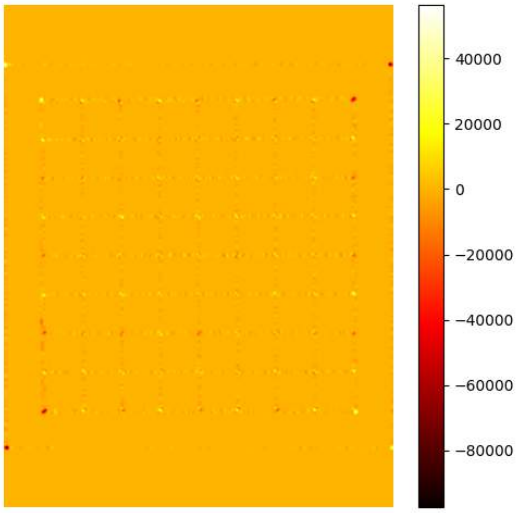

(c) The heatmap of S_{xy} represents the correlation between horizontal and vertical gradients, capturing regions with combined intensity changes in both directions. Notable responses appear at corner points, where gradients in the x- and y-directions interact, providing critical information for corner detection algorithms.

Figure 2: Visualization of the Structure Tensor Matrix components for the chessboard image(1).

3.2 Corner Response Function Q_{EG}

The matrix obtained has total edges, where the element on the main diagonal represents the energy edge in the directions of x and y, and the element on the minor diagonal represents the correlation along the edge in the x and y directions. The eigenvalues of this matrix indicate the strength of energy edges in the direction of the eigenvector of the matrix. Let λ be an eigenvalue of this matrix. Since it is a solution of

$$\begin{vmatrix} S_{xx} - \lambda & S_{xy} \\ S_{xy} & S_{yy} - \lambda \end{vmatrix} = (S_{xx} - \lambda)(S_{yy} - \lambda) - S_{xy}^2 = 0,$$

we have, $\lambda^2 - (S_{xx} + S_{yy})\lambda + S_{xx}S_{yy} - S_{xy}^2 = 0$. There are two eigenvalues, λ_1 and λ_2, which satisfy

$$\lambda_1 + \lambda_2 = S_{xx} + S_{yy} > 0, \quad \lambda_1\lambda_2 = S_{xx}S_{yy} - S_{xy}^2 > 0,$$

and the discriminant is

$$(S_{xx} + S_{yy})^2 - 4(S_{xx}S_{yy} - S_{xy}^2) = (S_{xx} - S_{yy})^2 + 4S_{xy}^2 \geq 0.$$

This implies that both λ_1 and λ_2 are real and nonnegative. In fact, λ_1 and λ_2 represent the variances of the two principal components of the (f_x, f_y) distribution. Using them, we can define the homogeneity measure Q_{EG} of the distribution by taking the ratio of the geometric mean of λ_1 and λ_2 to their arithmetic mean:

$$Q_{EG} = \left(\frac{\sqrt{\lambda_1\lambda_2}}{\frac{\lambda_1+\lambda_2}{2}} \right)^2 = \frac{4(S_{xx}S_{yy} - S_{xy}^2)}{(S_{xx} + S_{yy})^2}.$$

Since

$$0 \leq \sqrt{\lambda_1\lambda_2} \leq \frac{\lambda_1 + \lambda_2}{2} \quad (\lambda_1, \lambda_2 > 0),$$

this concludes the formulation. Q_{EG} is dimensionless and normalized such that:

$$0 \leq Q_{EG} \leq 1$$

Q_{EG} reaches 1 when the grayness variation is omnidirectional, in the sense that: $S_{xx} = S_{yy}$ and $S_{xy} = 0$ As the value of Q_{EG} approaches 1, the middle point of the window tends to become a corner. This method is applied to a matrix under the assumption that the minor diameters are equal elements and the eigenvalues of the matrix are positive. This is achievable by using the point multiplication of the gradient matrix in the x- and y-directions. To prevent the undefined condition where the value is indeterminate due to division by zero when the image is completely flat in Γ, it is useful to modify the definition of Q_{EG} as follows: since $S_{xx} \cdot S_{yy}$ represents the total variance of the gradient in Γ, we add a small constant σ_{EG}^4 to the denominator such that:

$$Q_{EG} = \frac{4(S_{xx}S_{yy} - S_{xy}^2)}{(S_{xx} + S_{yy})^2 + \sigma_{EG}^4}$$

This modification removes the undefined condition division by zero, with this adjustment, Q_{EG} is forced to be zero if $S_{xx} \cdot S_{yy}$ is significantly smaller than σ_{EG}^4. Therefore, σ_{EG}^4 acts as a threshold value for the grayness variation, which Q_{EG} classifies.

The results for Q_{EG} highlight its effectiveness in detecting corner points, with the method successfully identifying **85 corners** on the chessboard image (3a). The detected corners, marked in red, align precisely with the grid intersections, showcasing the robustness of Q_{EG} in capturing high-intensity gradient variations. The heatmap (3b) illustrates the spatial distribution of Q_{EG} values, where brighter regions correspond to corners with strong responses, while darker regions represent edges or flat areas. This visualization emphasizes Q_{EG}'s ability to differentiate corners from other features. The 3D surface plot (3c) complements these observations by showing sharp peaks at corner locations, indicating regions of high isotropic gradient variations. The smooth gradient transitions in other areas further validate Q_{EG}'s capacity to consistently distinguish corners from edges and flat regions.

(a) Detected corners using Q_{EG} on the chessboard image. Red markers indicate regions where Q_{EG} achieves high values, corresponding to strong corner responses.

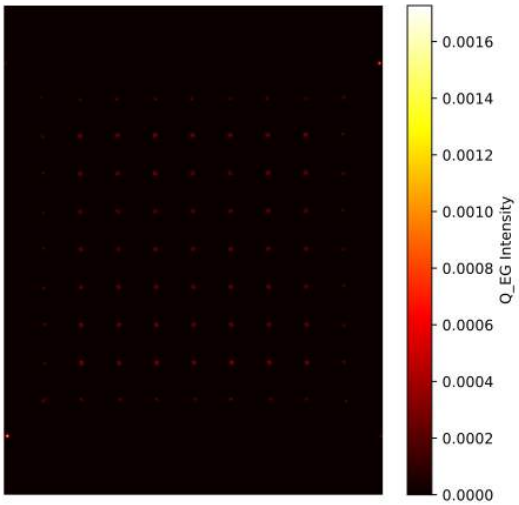

(b) Heatmap of Q_{EG} values across the chessboard image. Bright regions represent areas with high Q_{EG} values, indicating significant corner responses, while darker areas correspond to edges or flat regions.

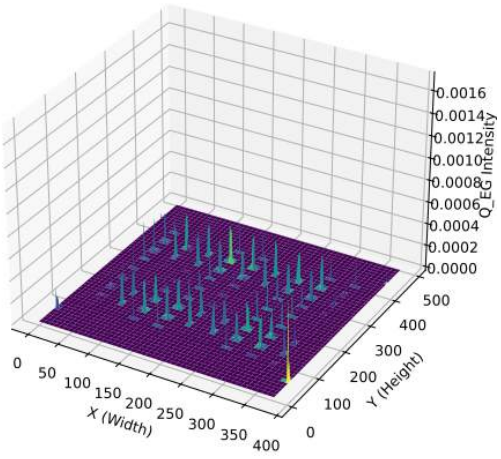

(c) 3D surface plot of Q_{EG} values across the chessboard image. The height of the surface represents the intensity of Q_{EG}, with peaks corresponding to corners and lower regions representing edges or flat areas.

Figure 3: Visualization of Q_{EG} applied to a chessboard image(1), showing the original image, 85 detected corners, a heatmap of Q_{EG} values highlighting corners, and a 3D surface plot illustrating the intensity distribution of Q_{EG}.

3.3 Corner Response Function Q_s

The corner response function Q_s is a mathematically robust measure designed to identify corner points in images by leveraging the squared structure tensor matrix $\hat{\mathbf{S}}$, defined as $\hat{\mathbf{S}} = \mathbf{S}^\top \mathbf{S} = \mathbf{S}^2$. Here, $\mathbf{S}$ represents the original structure tensor matrix, which discussed in section [3.1]. By squaring $\mathbf{S}$, the response to higher-order gradient variations is amplified, enhancing the ability to distinguish corners from edges and flat regions.The squaring operation emphasizes differences in gradient properties because $\mathbf{S}$ is symmetric ($\mathbf{S} = \mathbf{S}^\top$), ensuring $\hat{\mathbf{S}}$ highlights areas with high-intensity gradient interplay, which are indicative of corner features.

To define Q_s, two quantities δ_1 and δ_2 are introduced. These metrics are derived from the eigenvalues λ_1 and λ_2 of $\hat{\mathbf{S}}$, where $\lambda_1 \geq \lambda_2 \geq 0$. The eigenvalues represent dominant gradient variations, and their influence on δ_1 and δ_2 is expressed as:

$$\delta_1 = \sqrt{\lambda_1 \cdot \det(\hat{\mathbf{S}}^\top \hat{\mathbf{S}})}, \quad \delta_2 = \sqrt{\lambda_2 \cdot \det(\hat{\mathbf{S}}^\top \hat{\mathbf{S}})}.$$

Given that $\hat{\mathbf{S}}$ is symmetric, its determinant simplifies to $\det(\hat{\mathbf{S}}^\top \hat{\mathbf{S}}) = \det(\hat{\mathbf{S}}^2) = [\det(\hat{\mathbf{S}})]^2$, where $\det(\hat{\mathbf{S}}) = \lambda_1 \lambda_2$. This determinant represents the area-scaling factor of $\hat{\mathbf{S}}$, reflecting the spread of gradient information across regions of interest. δ_1 and δ_2, therefore, combine the magnitude and distribution of gradients, making them critical in capturing corner characteristics. The relationship between δ_1 and δ_2 is analyzed to validate the boundedness and consistency of Q_s. Using the squared difference property:

$$(\delta_1 - \delta_2)^2 \geq 0 \quad \Rightarrow \quad \delta_1^2 + \delta_2^2 \geq 2\delta_1 \delta_2,$$

and applying the Arithmetic-Geometric Mean inequality:

$$\delta_1 + \delta_2 \geq 2\sqrt{\delta_1 \delta_2}.$$

This ensures the normalized ratio, defined as:

$$Q_s = \frac{2\sqrt{\delta_1 \delta_2}}{\delta_1 + \delta_2},$$

is bounded between 0 and 1. Specifically, Q_s approaches 1 when $\delta_1 = \delta_2$, indicating isotropic gradient variations typical of corner points. Conversely, Q_s approaches 0 when $\delta_1 \gg \delta_2$ or $\delta_2 \gg \delta_1$, signifying edge-like or flat regions. This boundedness is critical for ensuring Q_s provides a consistent measure of corner strength across varying image conditions.

The results for Q_s highlight its effectiveness in identifying corner points by leveraging the squared structure tensor matrix. In the original chessboard image (1), the structured arrangement provides an excellent test case for corner detection. The detected corners visualization (4a) demonstrates Q_s's ability to successfully identify **85 significant corner points**, shown by the red markers, which align precisely with the intersections of the chessboard grid. The heatmap (4b) visualizes the distribution of Q_s values, with brighter regions indicating higher corner response values, effectively emphasizing corners while suppressing flat or edge-like regions. This demonstrates Q_s's capability to amplify higher-order gradient variations, providing robust corner detection even in complex gradient scenarios. The 3D surface plot (4c) further supports this observation by displaying distinct peaks at corner points, representing areas of high isotropic gradient variations. The smooth yet localized nature of the response confirms Q_s's ability to maintain consistency across different gradient magnitudes, making it a robust choice for corner detection in structured images like the chessboard. These visualizations collectively validate the mathematical foundation and practical effectiveness of Q_s.

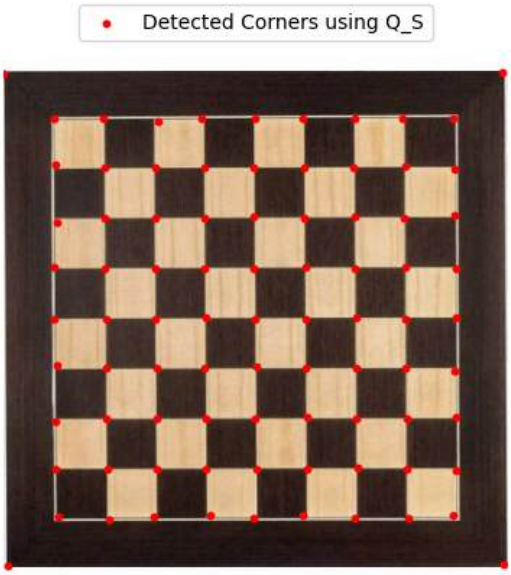

(a) Detected corners using Q_s on the chessboard image. Red markers indicate regions where Q_s achieves high values, corresponding to strong corner responses.

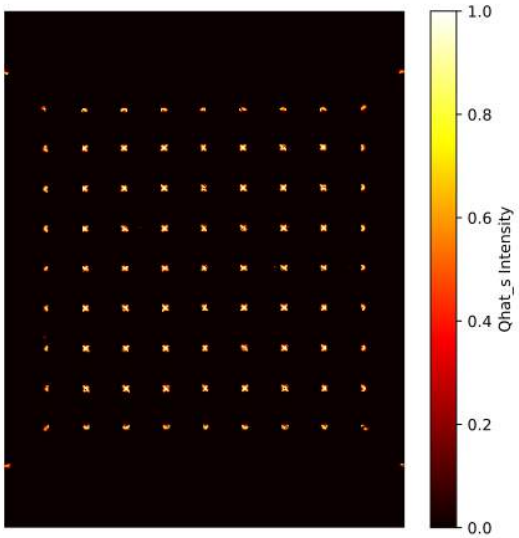

(b) Heatmap of Q_s values across the chessboard image. Bright regions represent areas with high Q_s values, indicating significant corner responses, while darker areas correspond to edges or flat regions.

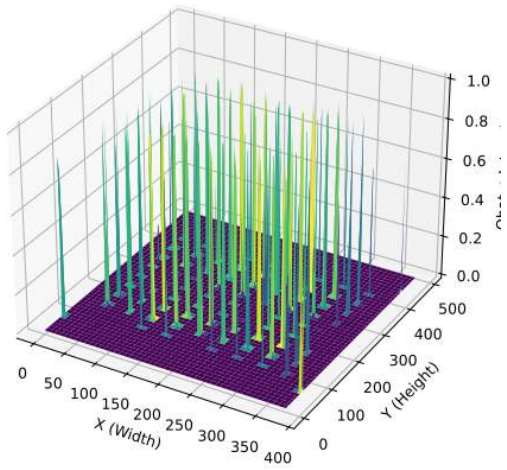

(c) 3D surface plot of Q_s values across the chessboard image. The height of the surface represents the intensity of Q_s, with peaks corresponding to corners and lower regions representing edges or flat areas.

Figure 4: Visualization of Q_s applied to a chessboard image(1), showing the original image, detected corners, a heatmap of Q_s values highlighting corners, and a 3D surface plot illustrating the intensity distribution of Q_s.

3.4 Corner Response Function Q_H

The Q_H feature extends existing corner response functions, leveraging the Heinz mean to enhance flexibility and robustness in evaluating gradient isotropy within a local neighborhood. By introducing a tunable parameter ν, the Heinz mean interpolates between the geometric and arithmetic means, enabling adjustable sensitivity to corner detection. As previously discussed in Section [3.1], the structure tensor $\mathbf{S}(i, j)$ provides a robust representation of local gradient variations. The Q_H feature is defined as the ratio of the geometric mean to the Heinz mean of the eigenvalues:

$$Q_H = \frac{\sqrt{\lambda_1 \lambda_2}}{H_\nu(\lambda_1, \lambda_2)},$$

where the Heinz mean $H_\nu(\lambda_1, \lambda_2)$ is given by:

$$H_\nu(\lambda_1, \lambda_2) = \frac{1}{2}\left(\lambda_1^{1-\nu}\lambda_2^{\nu} + \lambda_1^{\nu}\lambda_2^{1-\nu}\right), \quad 0 \leq \nu \leq 1.$$

This ratio satisfies $0 \leq Q_H \leq 1$, ensuring consistency across varying image conditions. Alternatively, the Q_H feature can be defined by normalizing the Heinz mean using the arithmetic mean:

$$Q_H = \frac{H_\nu(\lambda_1, \lambda_2)}{\frac{\lambda_1+\lambda_2}{2}},$$

where the arithmetic mean $\frac{\lambda_1+\lambda_2}{2}$ represents the average intensity variation. Since $H_\nu(\lambda_1, \lambda_2) \leq \frac{\lambda_1+\lambda_2}{2}$, this ratio also ensures $0 \leq Q_H \leq 1$.

The Q_H feature quantifies gradient isotropy in a neighborhood. It approaches 1 for isotropic gradients ($\lambda_1 \approx \lambda_2$), characteristic of corners, while it is significantly less than 1 for anisotropic gradients ($\lambda_1 \gg \lambda_2$ or $\lambda_2 \gg \lambda_1$), typical of edges. For flat regions ($\lambda_1 \approx \lambda_2 \approx 0$), Q_H nears 0.

The Q_H feature complements Q_{EG} by incorporating the Heinz mean's tunable sensitivity. While Q_{EG} emphasizes the overall variance and energy of gradients, Q_H introduces flexibility in characterizing isotropy through the parameter ν. Setting $\nu = \frac{1}{2}$ aligns Q_H with the geometric mean, paralleling Q_{EG}'s normalization. Using the arithmetic mean in Q_H provides an alternative perspective, balancing the influence of eigenvalues and further enhancing robustness in detecting isotropic regions.

The Q_H feature, as illustrated in the provided results, demonstrates the robustness and flexibility of corner detection through the use of the Heinz mean. The results depict two implementations of Q_H: one normalized by the arithmetic mean and the other by the geometric mean. Both approaches emphasize gradient isotropy, with Q_H nearing 1 in isotropic regions indicative of corners, as observed in the chessboard image. The detected corners (marked in red) align well with the expected corner locations, validating the method's accuracy. In both cases, a total of 85 corners were successfully detected, confirming the consistency and reliability of the method. The heatmaps illustrate the distribution of Q_H, with bright regions corresponding to strong corner responses and dark regions highlighting flat or edge areas. Notably, the arithmetic mean-based Q_H highlights broader corner regions due to its higher sensitivity to variations, while the geometric mean-based Q_H provides sharper localization, focusing on stronger corner regions. The 3D surface plots further corroborate these findings, with prominent peaks at corner locations and a near-zero response in flat regions, showcasing the method's ability to suppress noise and anisotropic gradients effectively. These results underscore the adaptability of Q_H, where the parameter ν enables a transition between sensitivity and specificity, making it suitable for various image conditions and corner types.

(a) Detected corners using Q_H with the arithmetic mean on the chessboard image. Red markers indicate regions where Q_H achieves high values, corresponding to strong corner responses.

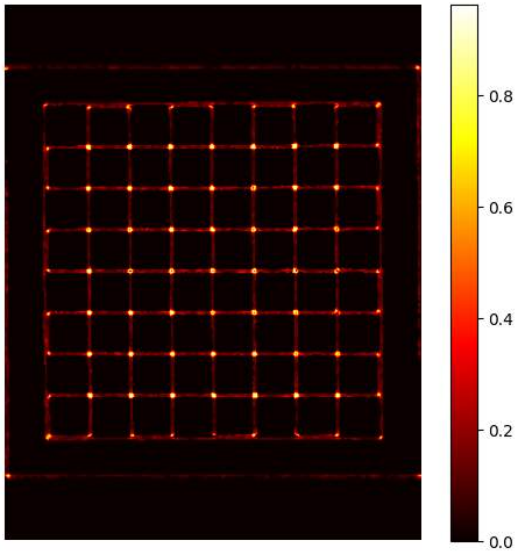

(b) Heatmap of Q_H values across the chessboard image. Bright regions represent areas with high Q_H values, indicating significant corner responses, while darker regions correspond to edges or flat regions.

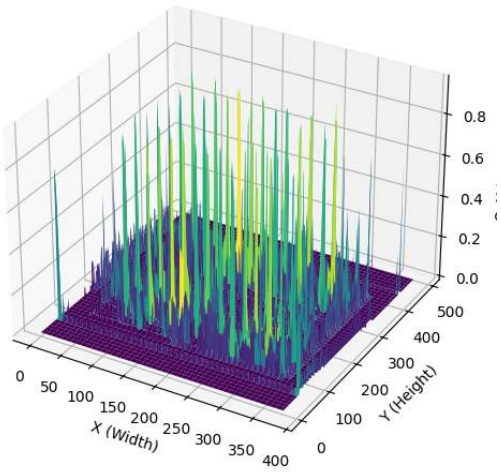

(c) 3D surface plot of Q_H values using the arithmetic mean across the chessboard image. The height of the surface represents the intensity of Q_H, with peaks corresponding to corners and lower regions representing edges or flat areas.

Figure 5: Visualization of Q_H (arithmetic mean) applied to a chessboard image(1), showing the original image, detected corners, a heatmap of Q_H values highlighting corners, and a 3D surface plot illustrating the intensity distribution of Q_H.

(a) Detected corners using Q_H with the geometric mean on the chessboard image. Red markers indicate regions where Q_H achieves high values, corresponding to strong corner responses.

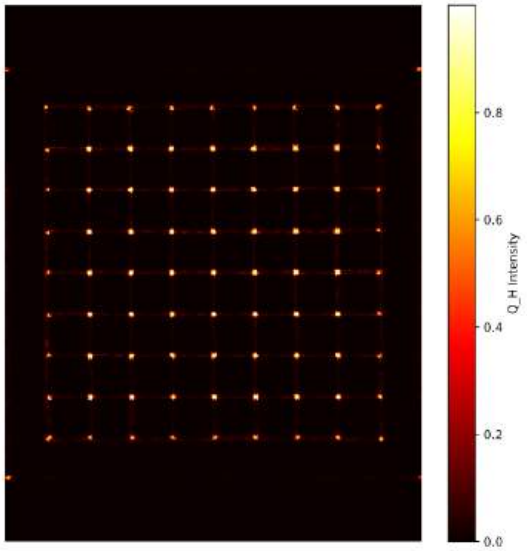

(b) Heatmap of Q_H values using the geometric mean across the chessboard image. Bright regions represent areas with high Q_H values, indicating significant corner responses, while darker regions correspond to edges or flat regions.

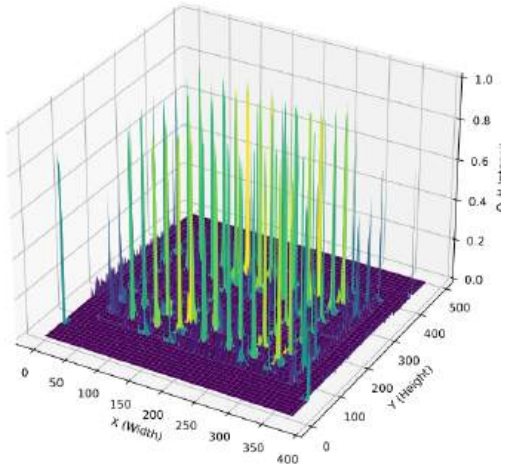

(c) 3D surface plot of Q_H values using the geometric mean across the chessboard image. The height of the surface represents the intensity of Q_H, with peaks corresponding to corners and lower regions representing edges or flat areas.

Figure 6: Visualization of Q_H (geometric mean) applied to a chessboard image(1), showing the original image, detected corners, a heatmap of Q_H values highlighting corners, and a 3D surface plot illustrating the intensity distribution of Q_H.

4 The Proposed algorithms

This section introduces three novel algorithms **Q_{EG}-based, Q_s-based, and Q_H-based corner detection** methods—designed to enhance the precision and robustness of corner detection in digital images. These algorithms are developed within the structure tensor framework and incorporate advanced mathematical formulations to evaluate gradient isotropy, energy distribution, and local intensity variations. Each method integrates smoothing, gradient analysis, adaptive thresholding, and non-maximum suppression (NMS) to balance noise resilience with sensitivity to fine image details. The distinctive feature of these algorithms lies in their flexibility, enabled by tunable parameters that adapt to diverse imaging conditions and application requirements. Detailed formulations and implementation steps for each algorithm are presented, highlighting their theoretical foundations and practical considerations for robust corner detection in complex visual environments.

4.1 Q_{EG} Based Corner Detection Algorithm

In this subsection, we propose an algorithm based on the Q_{EG} corner response function to detect corner points by leveraging isotropic gradient energy analysis. The method incorporates Gaussian smoothing, gradient computation, local gradient analysis, gradient energy thresholding, and non-maximum suppression (NMS) to optimize both accuracy and robustness.

The algorithm begins with *Gaussian smoothing* to suppress noise and stabilize gradient computations. A Gaussian filter with kernel size k and standard deviation σ is applied to the image. These parameters play critical roles in balancing noise reduction and detail preservation, as discussed in Section[3.1].

Following smoothing, *intensity gradients* in the x- and y-directions (f_x, f_y) are computed using Scharr operators, chosen for their precision and stability. The gradient magnitude is then computed as:

$$G(x, y) = |f_x + f_y|$$

An *adaptive threshold* is applied to $G(x, y)$, defined as:

$$T_G(x, y) = \alpha \cdot \overline{G}(x, y)$$

where $\overline{G}(x, y)$ is the local average gradient magnitude, and $\alpha \in (0, 1)$ is a scaling factor.

Similarly, the algorithm computes the gradient energy $E(x, y) = S_{xx}(x, y) + S_{yy}(x, y)$ and applies a fixed *gradient energy threshold* T_{energy}:

$$E(x, y) \geq T_{\text{energy}}$$

Only pixels satisfying both thresholds are retained for further analysis, while others are discarded. This ensures the algorithm focuses on significant local intensity variations with high gradient energy, improving computational efficiency by ignoring weak or noisy features. We compute Q_{EG} only for these pixels.

The Q_{EG} corner response function is then computed for these filtered regions, measuring the isotropy of gradient energy. A small stabilization constant (σ_{EG}^4) is incorporated to prevent division by zero in flat regions and to control sensitivity to low-gradient features. The computed Q_{EG} values highlight regions with high isotropic gradient energy, indicating potential corner points.

To further refine the Q_{EG} map, a global threshold is applied:

$$Q_{EG}(x, y) \geq T_{Q_{EG}}$$

where $T_{Q_{EG}}$ is a fixed value determined based on the desired sensitivity and characteristics of the application. This ensures that only prominent corner responses are kept, while noise and weaker features are excluded.

Finally, *non-maximum suppression (NMS)* is performed on the Q_{EG} map to identify local maxima within a predefined neighborhood. This step eliminates redundant detections, ensuring that the detected corners are distinct and well-localized. The size of the NMS window determines the spatial resolution of corner detection, with larger windows reducing redundancy and smaller windows preserving finer details.

4.2 Q_s Based Corner Detection Algorithm

In this subsection, we introduce an algorithm based on the Q_s corner response function. This method integrates Gaussian smoothing, gradient computation, adaptive thresholding, higher-order gradient analysis, and non-maximum suppression (NMS) to achieve robust and accurate corner detection.

The algorithm begins with *Gaussian smoothing* to reduce noise and stabilize the computation of gradients. A Gaussian filter with kernel size k and standard deviation σ is applied to the input image. These parameters are crucial for balancing noise suppression and the preservation of image details, as discussed in Section[3.1].

After smoothing, the *intensity gradients* in the x- and y-directions (f_x, f_y) are calculated using Scharr operators, which are known for their accuracy in edge detection. The gradient magnitude is then computed as:

$$G(x, y) = |f_x + f_y|$$

An *adaptive threshold* is applied to $G(x, y)$, defined as:

$$T_G(x, y) = \alpha \cdot \overline{G}(x, y)$$

where $\overline{G}(x, y)$ is the local average of the gradient magnitude, and $\alpha \in (0, 1)$ is a scaling factor.

Similarly, the algorithm computes higher-order gradient metrics $\delta_1(x, y)$ and $\delta_2(x, y)$, derived from the squared structure tensor. A fixed *delta threshold* T_δ is then applied:

$$\delta_1(x, y) \geq T_\delta \quad \text{and} \quad \delta_2(x, y) \geq T_\delta$$

Only pixels satisfying both thresholds are retained for further analysis, while others are discarded. This ensures the algorithm focuses on regions with significant local intensity variations and strong higher-order gradient responses, improving computational efficiency by ignoring weak or noisy features. We compute Q_s only for these pixels.

The Q_s corner response function is then computed for the filtered pixels, measuring the isotropy of higher-order gradient variations. A global threshold T_s is applied:

$$Q_s(x, y) \geq T_s$$

where T_s is a fixed value determined based on the desired sensitivity and application requirements. This ensures that only prominent corner responses are kept, while noise and weaker features are excluded.

Finally, *non-maximum suppression (NMS)* is performed on the Q_s map to identify local maxima within a predefined neighborhood. This step eliminates redundant detections, ensuring that the detected corners are distinct and well-localized. The size of the NMS window affects the spatial resolution of corner detection, with larger windows reducing redundancy and smaller windows preserving finer details.

4.3 Q_H Based Corner Detection Algorithm

The Q_H-based corner detection algorithm leverages multiple thresholds to robustly identify corner points by analyzing isotropic gradient energy and applying adaptive filtering techniques. The algorithm begins with *Gaussian smoothing*, which suppresses noise and stabilizes gradient computations. A Gaussian filter with kernel size k and standard deviation σ is applied to the image to ensure consistent processing of local intensity variations.

After smoothing, *intensity gradients* (f_x, f_y) are computed using Scharr operators for their precision and stability. The gradient magnitude is then computed as:

$$G(x, y) = |f_x + f_y|$$

An *adaptive gradient magnitude threshold* is applied. The local average gradient magnitude $\overline{G}(x, y)$ is computed over a specified neighborhood. The adaptive threshold is defined as:

$$T_G(x, y) = \alpha \cdot \overline{G}(x, y)$$

where $\alpha \in (0, 1)$ is a scaling factor. Pixels satisfying:

$$G(x, y) \geq T_G(x, y)$$

are retained for further processing, while others are discarded. This step ensures the algorithm adapts to local variations in intensity, focusing on significant gradient changes while suppressing noise and weak features. For the retained pixels, the algorithm computes the gradient energy $E(x, y) = S_{xx}(x, y) + S_{yy}(x, y)$. A fixed *gradient energy threshold* T_{energy} is then applied:

$$E(x, y) \geq T_{\text{energy}}$$

This ensures the algorithm focuses on high-energy regions likely to contain corner points.

The Q_H corner response function is then computed for these filtered pixels. To retain only significant corner responses, a *global threshold* is applied:

$$Q_H(x, y) \geq T_H$$

where T_H is a fixed value determined based on the desired sensitivity and characteristics of the application. This eliminates weaker Q_H values, ensuring only prominent corner points are considered.

Finally, *non-maximum suppression (NMS)* is performed on the Q_H map to identify local maxima within a predefined neighborhood. This step eliminates redundant detections, ensuring that the detected corners are distinct and well-localized. The NMS window size determines the spatial resolution of corner detection, with larger windows reducing redundancy and smaller windows preserving finer details.

Algorithm 1 Unified Framework for Proposed Corner Detection Algorithms

Step 1: Preprocessing

Smooth the input image I using a Gaussian filter with kernel size k and standard deviation σ:

$$I_{\text{smooth}} = \text{GaussianFilter}(I, k, \sigma)$$

Step 2: Gradient Computation

Compute intensity gradients f_x and f_y using Scharr operators:

$$f_x = \text{Scharr}(I_{\text{smooth}}, \text{direction} = \text{"}x\text{"}) \quad f_y = \text{Scharr}(I_{\text{smooth}}, \text{direction} = \text{"}y\text{"})$$

Optionally, compute the gradient magnitude:

$$|f_x + f_y|$$

Step 3: Structure Tensor Calculation

Compute the components of the structure tensor:

$$S_{xx} = f_x^2, \quad S_{xy} = f_x f_y, \quad S_{yy} = f_y^2$$

Smooth these components using a Gaussian filter:

$$S_{xx} = \text{GaussianFilter}(S_{xx}, k, \sigma), \quad S_{xy} = \text{GaussianFilter}(S_{xy}, k, \sigma), \quad S_{yy} = \text{GaussianFilter}(S_{yy}, k, \sigma)$$

Step 4: Eigenvalue Computation

Compute the eigenvalues λ_1 and λ_2 of the structure tensor:

$$\lambda_1, \lambda_2 = \text{Eigenvalues}(\mathbf{S}) \quad \text{where} \quad \mathbf{S} = \begin{bmatrix} S_{xx} & S_{xy} \\ S_{xy} & S_{yy} \end{bmatrix}$$

Step 5: Apply Local Average gradients and gradient energy Thresholding

Threshold based on local average gradients:

$$T_G(i,j) = \alpha \cdot \overline{G}(i,j),$$
$$\text{If } G(i,j) \geq T_G(i,j), \text{ then compute } Q(i,j),$$
$$\text{else set } Q(i,j) = 0.$$

Compute the gradient energy:

$$E(x,y) = S_{xx} + S_{yy}$$

Apply gradient energy threshold T_{energy}:

$$\text{Retain pixels where } E(x,y) \geq T_{\text{energy}}$$

Step 6: Compute corner response function

$$Q_{EG} = \frac{4(S_{xx}S_{yy} - S_{xy}^2)}{(S_{xx} + S_{yy})^2 + \sigma_{EG}^4}, \; Q_s = \frac{2\sqrt{\delta_1\delta_2}}{\delta_1 + \delta_2}, \; Q_H = \frac{\sqrt{\lambda_1\lambda_2}}{H_\nu(\lambda_1, \lambda_2)}, \; Q_H = \frac{H_\nu(\lambda_1, \lambda_2)}{\frac{\lambda_1+\lambda_2}{2}}$$

Step 7: Apply Global Thresholding

Apply a global threshold:

$$\text{Retain pixels where } Q(x,y) \geq T_{\text{Global}}$$

Step 8: Apply Non-Maximum Suppression (NMS)

Apply NMS within a window size w to refine corner localization and identify local maxima.

Return the list of detected corner coordinates.

5 Experimental Analysis and Performance Evaluation

The performance of the proposed corner detection algorithms (Q_{EG}, Q_s, Q_H) is evaluated using synthetic, real-world, and structured test images, focusing on three key contexts: a geometric structure image, the MNIST digit dataset, and two real-world examples—a garage image and a staircase image. The geometric structure image serves as a benchmark for detecting well-defined corners in repetitive patterns, while the MNIST dataset tests adaptability to irregular, curved shapes in handwritten digits. The garage image represents a cluttered real-world scene, and the staircase image provides a structured yet noisy setting with repetitive geometric features. The evaluation considers performance under normal conditions, noise (Gaussian and salt-and-pepper), and geometric transformations like rotation and shear. Among the algorithms, Q_H (Geometric Mean) demonstrates robustness, consistently performing well across diverse scenarios and under challenging conditions. The inclusion of real-world images enhances the analysis, ensuring a comprehensive understanding of the algorithms capabilities and limitations. Detailed results and visual examples are presented in subsequent sections.

5.1 Qualitative Results of Corner Detection

To thoroughly evaluate the performance of the proposed corner detection algorithms, we applied Q_{EG}, Q_H (arithmetic and geometric mean variants), and Q_s to two distinct datasets: the geometric structure image and the MNIST handwritten digits dataset. The geometric structure image, characterized by its dense array of intricate and repetitive patterns, serves as a challenging benchmark for corner detection due to its high corner density and complex arrangements. In contrast, the MNIST dataset provides a diverse set of handwritten digit images with varying corner features, ranging from sharp to rounded, offering a complementary evaluation scenario to assess the adaptability of the algorithms.

We start our experiment with the geometric structure image :

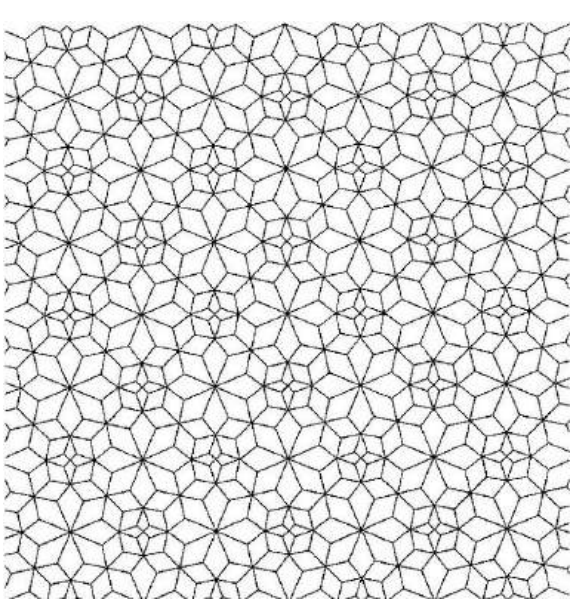

(a) Original Geometric Structure Image. The original geometric pattern is characterized by a high density of corners and intricate structures, providing a challenging benchmark for corner detection algorithms.

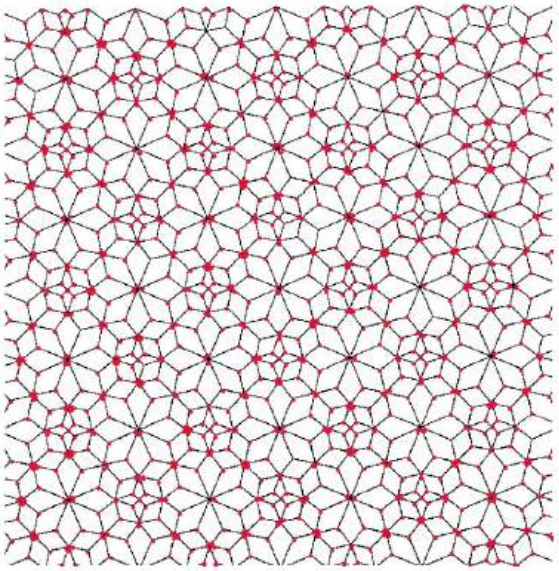

(b) Corners Detected Using Harris Method. The detected corners (marked in red) using the Harris corner detection algorithm. A total of 1460 corners were identified, demonstrating the method's sensitivity to high-frequency details in the pattern.

Figure 7: Original geometric structure and corners detected using the Harris corner detection method. The left subfigure illustrates the original geometric structure characterized by a high density of intricate patterns and corners. The right subfigure presents the corners detected (highlighted in red) using the Harris algorithm, showcasing its sensitivity to high-frequency details by identifying a total of 1460 corners.

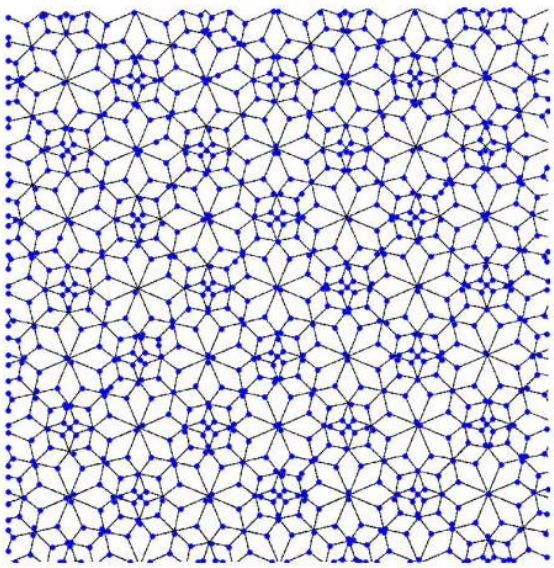

(a) Corners detected using Q_s on the geometric structure image. The method identifies 1000 corners, leveraging higher-order gradient interactions to enhance precision.

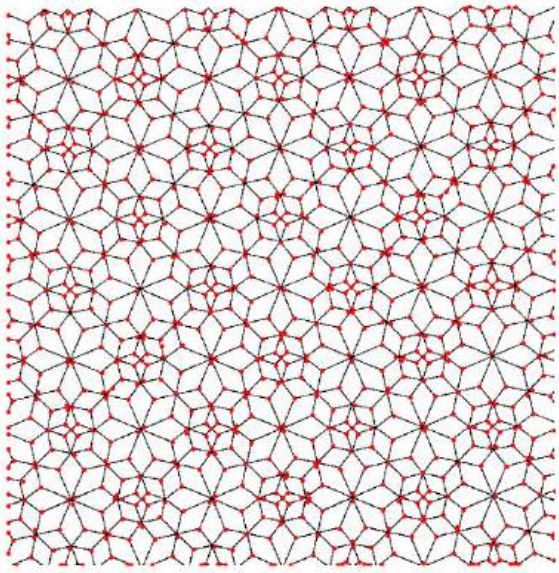

(b) Corners detected using Q_{EG} on the geometric structure image. The method successfully captures 1002 distinct corners, emphasizing areas with high isotropic gradient variations.

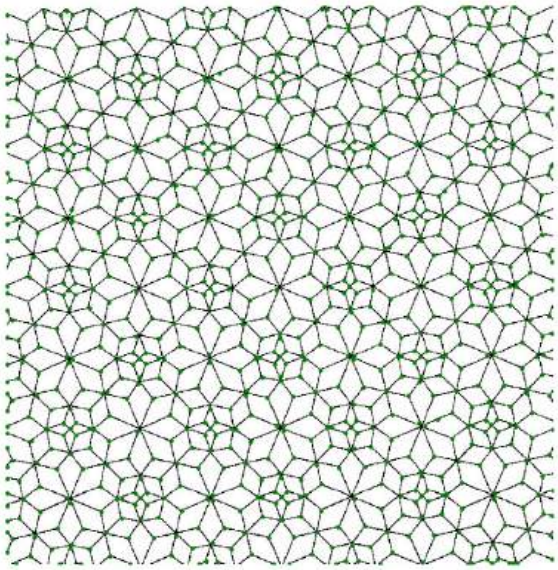

(c) Corners detected using Q_H with the arithmetic mean on the geometric structure image. A total of 899 corners are identified, showcasing the method's robustness to fine geometric patterns.

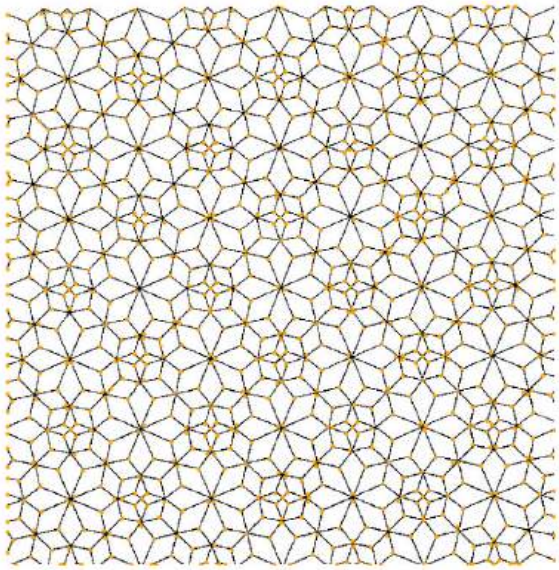

(d) Corners detected using Q_H with the geometric mean on the geometric structure image. This approach highlights 1002 corners, effectively balancing sensitivity and isotropy in complex structures.

Figure 8: Corners detected on the geometric structure image using various methods. The top left subfigure shows the detection using Q_s, which identifies 1000 corners by leveraging higher-order gradient interactions for precision. The top right subfigure illustrates the Q_{EG} method, detecting 1002 corners by emphasizing regions with high isotropic gradient variations. The bottom left subfigure presents results from Q_H using the arithmetic mean, detecting 899 corners and demonstrating robustness to intricate geometric patterns. Finally, the bottom right subfigure displays corners detected by Q_H with the geometric mean, highlighting 1002 corners with a balanced approach to sensitivity and isotropy in complex structures.

The results of corner detection on the geometric structure image using Q_{EG}, Q_H (arithmetic and geometric mean variants), Q_s, and the Harris method [6] reveal significant insights into their performance.The Harris method detected the highest number of corners (1460), showing a high sensitivity to fine details but at the cost of identifying redundant or less significant points in dense regions. Conversely, Q_{EG} and Q_H (geometric mean) detected 1000 and 1002 corners, effectively focusing on critical corner points with high isotropic gradient variations, reducing redundancy. Q_s detected 1000 corners, leveraging higher-order gradient interactions to maintain a balance between precision and coverage. The Q_H (arithmetic mean) variant detected fewer corners (899), emphasizing robustness over density, making it suitable for scenarios prioritizing cleaner corner maps.Compared to the Harris method, all Q-based metrics demonstrated better resilience to complex geometric patterns by avoiding over-detection and providing more structured corner distributions, aligning closely with critical points in the image.

Table 1: Algorithm Parameters for Geometric Structure Image

Parameter	**Harris**	Q_{EG}	Q_s	Q_H **(Arithmetic)**	Q_H **(Geometric)**
Number of Corners Detected	1460	1000	1000	899	1002
Block Size	6	-	-	-	-
Aperture Size (ksize)	3	-	-	-	-
Harris k	0.004	-	-	-	-
Threshold Ratio	0.44	-	-	-	-
Gaussian Kernel Size	-	3	3	3	3
Gaussian Sigma	-	0.999	0.999	0.999	0.999
Threshold	-	0.66	0.799	0.99111	0.81
Gradient Alpha	-	0.15	0.15	0.15	1.0
Gradient Energy Threshold	-	2000.0	9.99e+27	699000.0	990000.0
Sigma_{EG}	-	150.0	-	-	-
NMS Window Size	-	9	9	9	9
Heinz Mean Parameter (ν)	-	-	-	0.01	1

We continue our experiment using the MNIST dataset image :

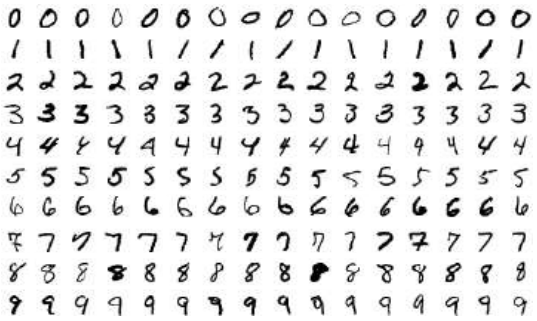

(a) Original MNIST dataset image showcasing a grid of handwritten digits ranging from 0 to 9, used as a benchmark for corner detection evaluation.

(b) Corners detected using Harris on the MNIST dataset. The method effectively identifies prominent corners,A total of 872 corners are detected.

(c) Corners detected using Q_s on the MNIST dataset. The method identifies 531 corners.

(d) Corners detected using Q_{EG} on the MNIST dataset. This method successfully captures 573 corners.

(e) Corners detected using Q_H with the arithmetic mean on the MNIST dataset. A total of 508 corners are identified.

(f) Corners detected using Q_H with the geometric mean on the MNIST dataset. This approach highlights 514 distinct corners.

Figure 9: Corner detection on the MNIST dataset using Q_s, Q_{EG}, and Q_H methods.

The corner detection results on the MNIST handwritten digit dataset showcase varying performance across the methods, reflecting their adaptability to diverse shapes and corner complexities. The Harris corner detection algorithm identifies 872 corners, demonstrating its capability to detect prominent corners but with potential over-detection in noisy or less-defined areas. The Q_{EG} method detects 573 corners, prioritizing high isotropic gradient variations, leading to more selective corner identification. Similarly, Q_H with the arithmetic mean captures 508 corners, emphasizing robustness to localized intensity variations, while Q_H with the geometric mean identifies 514 corners, balancing sensitivity to geometric features and gradient interactions. The Q_s algorithm detects 531 corners, effectively leveraging higher-order gradient terms to capture significant corner features, providing a trade-off between sensitivity and precision.

Table 2: Algorithm Parameters for MNIST Image

Parameter	**Harris**	Q_{EG}	Q_s	Q_H **(Arithmetic)**	Q_H **(Geometric)**
Number of Corners Detected	872	573	531	508	514
Block Size	6	-	-	-	-
Aperture Size (ksize)	5	-	-	-	-
Harris k	0.06	-	-	-	-
Threshold Ratio	0.15	-	-	-	-
Gaussian Kernel Size	-	3	3	3	3
Gaussian Sigma	-	0.999	0.99	0.9	0.9
Threshold	-	0.05	0.05	0.5	0.3
Gradient Alpha	-	0.15	0.15	0.1	1.0
Gradient Energy Threshold	-	35000.0	9.99e+23	1000000.0	900000.0
Sigma_{EG}	-	9000.0	-	-	-
NMS Window Size	-	9	9	9	9
Heinz Mean Parameter (ν)	-	-	-	0.3	1

5.2 Robustness to Noise

To rigorously assess the robustness of the proposed corner detection algorithms, experiments were conducted on images corrupted with two prevalent types of noise: Gaussian noise and salt-and-pepper noise. Gaussian noise was applied with standard deviations ($\sigma = 25$ and $\sigma = 35$), representing moderate to high noise levels. For salt-and-pepper noise, salt intensity ($p_{\text{salt}} = 0.009$ and $p_{\text{salt}} = 0.029$) and pepper intensity ($p_{\text{pepper}} = 0.009$ and $p_{\text{pepper}} = 0.029$) were applied, simulating real-world sensor or transmission artifacts. The staircase image dataset, characterized by its intricate geometric features, was used as a benchmark to analyze the performance of Harris, Q_{EG}, Q_H (arithmetic and geometric mean variants), and Q_s corner detection algorithms under these noisy conditions. The evaluation highlights the sensitivity, stability, and adaptability of the methods in detecting meaningful corner features despite varying noise intensities.

The evaluation of the corner detection algorithms under Gaussian and salt-and-pepper noise highlights significant differences in their robustness and accuracy. Among the tested methods, Q_H-geometric consistently outperforms the others, demonstrating superior resilience to noise and reliable corner detection, making it the most robust choice. The Q_s algorithm performs very well under Gaussian noise at both $\sigma = 25$ and $\sigma = 35$, effectively detecting corners with minimal interference from noise. This indicates that Q_s is adept at maintaining precision in relatively controlled noisy environments. However, Q_{EG} and Q_H-arithmetic, while detecting corners accurately, are susceptible to noise artifacts, particularly at higher noise levels. The Q_H-geometric algorithm, on the other hand, showcases exceptional noise suppression and accurate corner detection, emerging as the best-performing method under Gaussian noise. It maintains clean outputs without compromising detection quality, even at $\sigma = 35$. The Harris method also demonstrates robust performance, successfully detecting most corners. However, at higher noise levels, it occasionally misses some corners, indicating its slightly reduced resilience compared to Q_H-geometric.

The salt-and-pepper noise ($p = 0.009$ and $p = 0.029$) presents a more challenging scenario. Here, Q_s, Q_{EG}, and Q_H-arithmetic struggle significantly, with substantial noise artifacts and poor corner detection. Their performance deteriorates further as the noise intensity increases, indicating limited robustness to this noise type. In contrast, Q_H-geometric demonstrates remarkable resilience at $p = 0.009$, accurately detecting corners while suppressing noise to a significant degree. At the higher intensity of $p = 0.029$, its performance declines, with more noticeable noise interference, but it still maintains a clear edge over the other algorithms. The Harris method performs poorly under salt-and-pepper noise, failing to suppress noise artifacts and detect corners accurately, making it unsuitable for such conditions.

Overall, Q_H-geometric emerges as the most robust algorithm, excelling in both Gaussian and salt-and-pepper noise scenarios. Its ability to suppress noise while preserving corner detection accuracy sets it apart, making it an ideal choice for noisy environments. Conversely, Q_s and Harris perform well under Gaussian noise but are less effective against salt-and-pepper noise, while Q_{EG} and Q_H-arithmetic exhibit significant limitations under both noise types.

Figure 10: Corner detection results on staircase images under varying noise types and intensities using multiple algorithms.

Noise Type	Q_H**-Geometric**	Q_s	Q_{EG}	Q_H**-Arithmetic**	**Harris**
Gaussian Noise ($\sigma = 25$)	Excellent	Very Good	Moderate	Moderate	Good
Gaussian Noise ($\sigma = 35$)	Excellent	Good	Poor	Poor	Moderate
Salt-and-Pepper ($p = 0.009$)	Very Good	Poor	Poor	Poor	Poor
Salt-and-Pepper ($p = 0.029$)	Moderate	Very Poor	Very Poor	Very Poor	Very Poor

Table 3: Performance Evaluation of Corner Detection Algorithms under Gaussian and Salt-and-Pepper Noise.

5.3 Invariance to Geometric Transformations

This subsection evaluates the robustness of the proposed corner detection algorithms under geometric transformations, specifically 180-degree rotation and shear. Unlike synthetic test patterns often used in such studies, the analyzed images are derived from real-world scenarios, adding complexity and practical relevance to the evaluation. The objective is to determine the consistency of corner detection results when images are subjected to these transformations, which are commonly encountered in various real-world applications. The analysis focuses on four algorithms—Q_{EG}, Q_s, Q_H (Arithmetic Mean), and Q_H (Geometric Mean)—to assess their performance under these changes. For the 180-degree rotation, all algorithms demonstrated exceptional robustness. The number of detected corners remained identical to the original image, indicating perfect invariance to rotation. This consistency underscores the rotational symmetry embedded in the mathematical structures of the algorithms, ensuring that corners are reliably detected irrespective of the image's orientation. Such invariance is critical in real-world applications like object recognition or visual tracking, where rotated objects are frequently encountered. These results affirm the algorithms' suitability for scenarios requiring rotation-insensitive corner detection. The performance under shear transformation presented a slightly different picture. While the algorithms maintained general consistency, minor variations in the number of detected corners were observed. For Q_s, the number of corners increased slightly from 277 in the original image to 282 after the shear transformation, showcasing its robustness with minimal sensitivity to structural distortions. Similarly, Q_{EG} exhibited a small increase from 268 to 283, demonstrating its ability to adapt to subtle changes while maintaining reliable detection. Q_H (Arithmetic Mean) showed a slightly higher sensitivity, with the number of detected corners increasing from 358 to 365. This behavior suggests that the arithmetic mean variant is more responsive to localized intensity variations induced by the shear transformation. On the other hand, Q_H (Geometric Mean) displayed remarkable stability, with the number of corners increasing only from 264 to 268, marking it as the most stable method under shear. The analysis highlights the overall resilience of these algorithms to geometric transformations. By using a real-world image for this evaluation, the findings emphasize the algorithms' potential for practical deployment in realistic environments, where such transformations are common.

Transformation	Q_s	Q_{EG}	Q_H (Arithmetic)	Q_H (Geometric)
Original Image	277	268	358	264
180-Degree Rotation	277	268	358	264
Shear Transformation	282	283	365	268
Change under Shear (+)	+5	+15	+7	+4

Table 4: Performance Evaluation of Proposed Corner Detection Algorithms under Geometric Transformations. Each column represents an algorithm, while the rows summarize results of number of detected corners for the original image, 180-degree rotation, and shear transformation. The last row shows the change in detected corners under shear.

(a) Original image

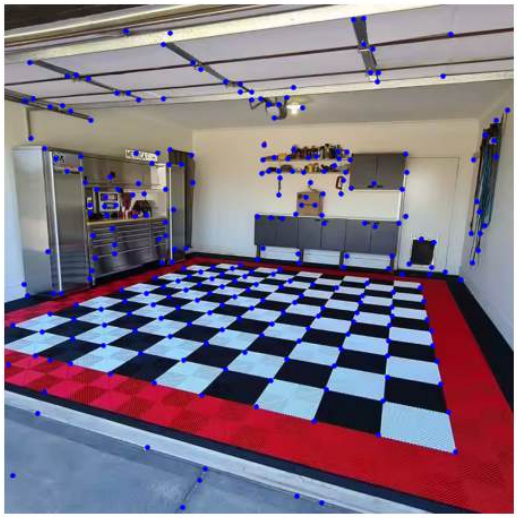

(b) Original image Q_S

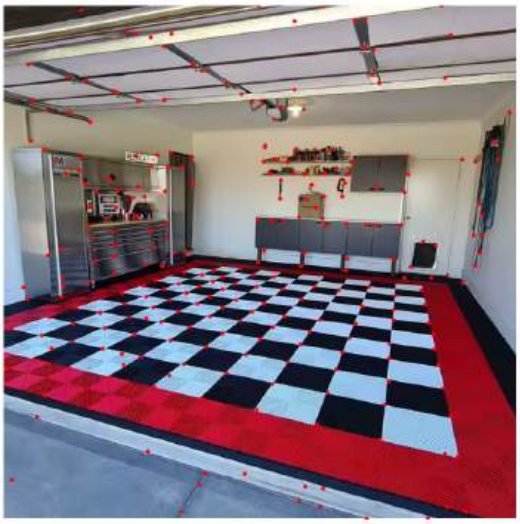

(c) Original image Q_EG

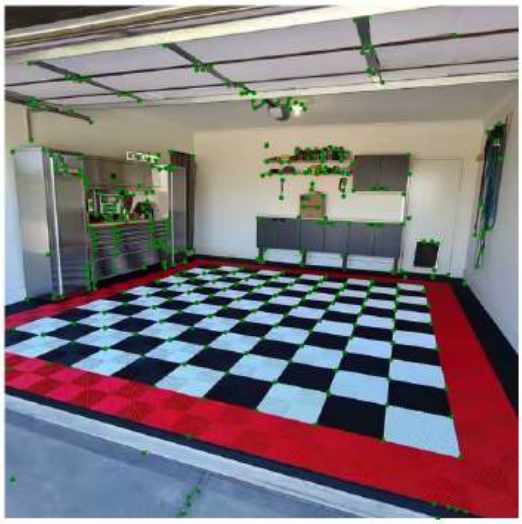

(d) Original image Q_H (Arithmatic)

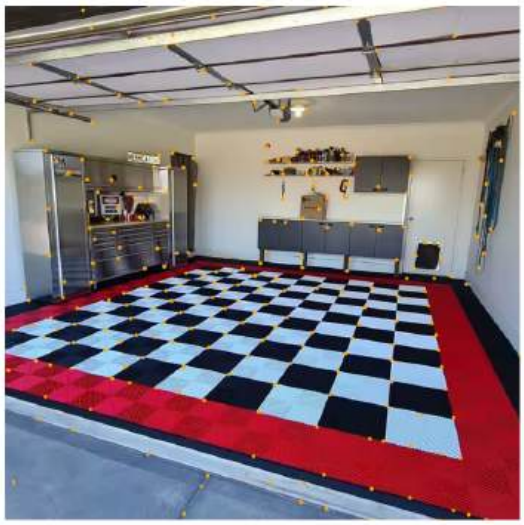

(e) Original image Q_H (Geometric)

Figure 11: Comparison of corner detection methods on the original image using Q_s, Q_{EG}, and Q_H with both arithmetic and geometric means.

(a) Original image - rotated

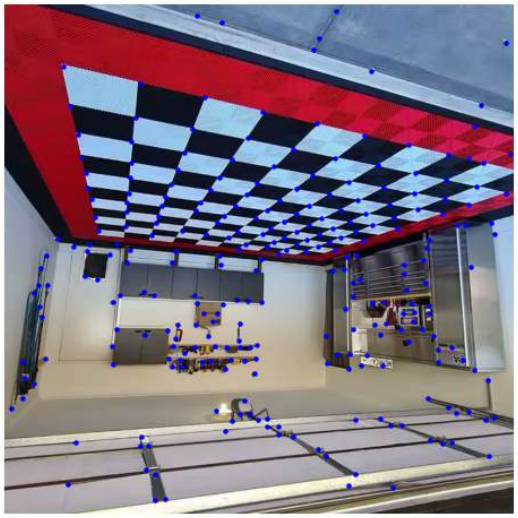

(b) Original image rotated Q_S

(c) Original image rotated Q_EG

(d) Original image rotated Q_H (Arithmetic)

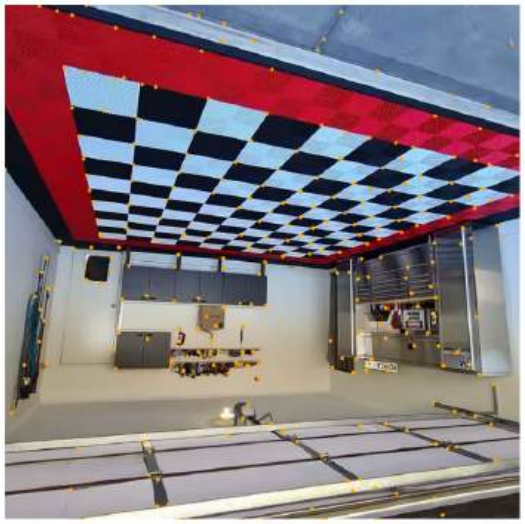

(e) Original image rotated Q_H (Geometric)

Figure 12: Corner detection on the rotated image using Q_s, Q_{EG}, and Q_H with arithmetic and geometric means.

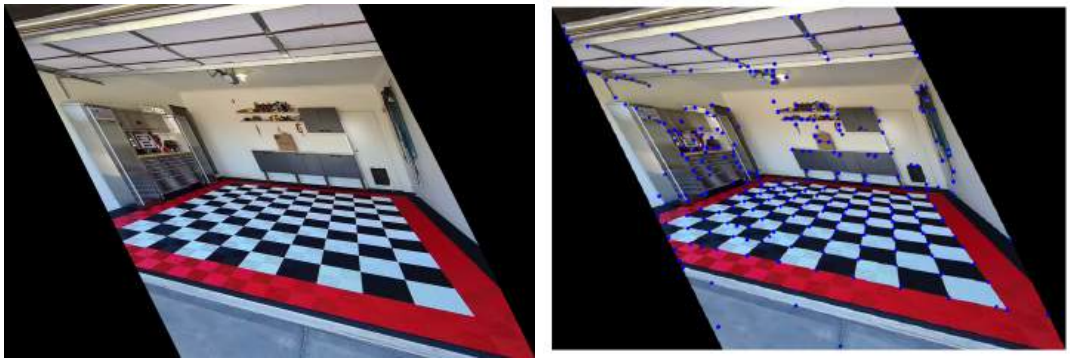

(a) Original image sheared

(b) Shear Q_S

(c) Shear Q_EG

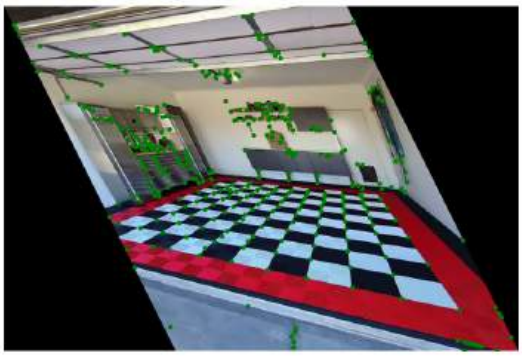

(d) Shear Q_H (Arithmetic)

(e) Shear Q_H (Geometric)

Figure 13: Corner detection on the sheared image using Q_s, Q_{EG}, and Q_H with arithmetic and geometric means.

6 Conclusion

In this paper, we introduced three novel corner detection methods based on the corner response functions Q_{EG}, Q_s, and Q_H, all grounded in the structure tensor framework. These methods aim to enhance the precision and robustness of corner detection by analyzing gradient isotropy, higher-order gradient interactions, and incorporating the flexibility of the Heinz mean. The Q_{EG} function emphasizes isotropy in gradient variations by utilizing the eigenvalues of the structure tensor matrix, providing a robust foundational approach for detecting corners in images with well-defined structures. The Q_s function leverages the squared structure tensor matrix to amplify higher-order gradient variations, enhancing sensitivity to subtle corner characteristics. The Q_H function introduces a tunable parameter ν via the Heinz mean, offering flexibility in balancing sensitivity and robustness, allowing it to adapt to specific corner detection needs. Our experimental analysis demonstrated that all three proposed methods effectively detect corners in both structured geometric images and natural images like those from the MNIST dataset. The Q_H function, especially with the geometric mean, exhibited exceptional resilience to both Gaussian and salt-and-pepper noise, outperforming other methods in challenging scenarios. The algorithms were also tested for invariance to geometric transformations such as rotation and shear. The results confirmed that the proposed methods maintain consistent corner detection performance under these transformations, highlighting their applicability in real-world situations where images may be rotated or distorted. In conclusion, the proposed corner detection algorithms provide a solid foundation for accurate and reliable corner detection in various imaging conditions. They offer advantages in adaptability, robustness to noise, and invariance to geometric transformations, making them suitable for a wide range of computer vision applications, including feature extraction, pattern recognition, and image registration. Future work will focus on optimizing these algorithms for real-time applications. Additionally, integrating these methods with machine learning frameworks could further enhance their performance and open up new possibilities in advanced image processing tasks.

References

[1] A review of corner detection algorithms based on image contour. In *2020 5th International Conference on Intelligent Informatics and Biomedical Sciences (ICIIBMS)*. IEEE, Nov 2020. Date added to IEEE Xplore: 02 February 2021.

[2] Fereshteh Behbahani, Alireza Behrad, and Mohammad Hossein Moaiyeri. An ultra-fast and energy-efficient cntfet-based image corner detection hardware for real-time image processing applications. *AEÜ - International Journal of Electronics and Communications*, 175:155099, 2024.

[3] Luca Bertinetto, Jack Valmadre, João F. Henriques, Andrea Vedaldi, and Philip H. S. Torr. Fully-convolutional siamese networks for object tracking, 2021.

[4] Fei Du, Peng Liu, Wei Zhao, and Xianglong Tang. Correlation-guided attention for corner detection based visual tracking. pages 6835–6844, 2020.

[5] W. Förstner and E. Gülch. A fast operator for detection and precise location of distinct points, corners and centres of circular features. In *ISPRS Proceedings*, 1987.

[6] Chris Harris and Mike Stephens. A combined corner and edge detector. In *Alvey Vision Conference*, pages 147–151, 1988.

[7] Tushar Hrishikesh Jaware, Vinodkumar Ramesh Patil, Chittaranjan Nayak, Ali Elmasri, Nawaf Ali, and Purnendu Mishra. A novel approach for brain tissue segmentation and classification in infants' mri images based on seeded region growing, foster corner detection theory, and sparse autoencoder. *Alexandria Engineering Journal*, 76:289–305, August 2023.

[8] Baptiste Magnier and Khizar Hayat. Revisiting mehrotra and nichani's corner detection method for improvement with truncated anisotropic gaussian filtering. *Sensors*, 23:8653, 2023.

[9] Baptiste Magnier and Khizar Hayat. Revisiting mehrotra and nichani's corner detection method for improvement with truncated anisotropic gaussian filtering. *Sensors*, 23(20):8653, 2023.

[10] Xiang Pan, Jing Zhu, Hongbin Yu, Lifang Chen, Yuan Liu, and Lihua Li. Robust corner detection with fractional calculus for magnetic resonance imaging. *Biomedical Signal Processing and Control*, 63:102112, 2021.

[11] Yi-Chuang Wu, Yi-Chen Liang, Yung-Hsing Liu, Yong-Sheng Chen, Bishnu Nand Yadav, and Hang-Suin Yang. The measurement of pressure-volume diagram of a flat alpha-type stirling engine based on laser triangulation and hybrid harris corner methods. *Results in Engineering*, 21:101877, 2024.

[12] Reza Yazdi and Hassan Khotanlou. Robust corner detector based on local maximum and minimum differences. In *2024 10th International Conference on Web Research (ICWR)*, pages 92–98, 2024.

[13] Nan Zhang, Shupeng Han, Xiaoming Chen, Haodong Chen, Li Tan, and Yuk Ying Chung. Event vision-based corner detection with count-normalized multi-layer perceptron and throughput indicator. *Computers and Electrical Engineering*, 118, Part B:109432, September 2024.

[14] Wei Zhu et al. Sub-pixel checkerboard corner localization for robust vision measurement. *IEEE Signal Processing Letters*, 31:21–25, December 2023.

Declarations

List of Abbreviations

- Q_{EG}: Corner response function based on eigenvalues of the structure tensor matrix.
- Q_s: Corner response function leveraging the squared structure tensor.
- Q_H: Corner response function incorporating the Heinz mean.
- NMS: Non-Maximum Suppression.

Ethics Approval and Consent to Participate

Not applicable. This study does not involve human participants, human data, human tissue, animals, or plants.

Consent for Publication

Not applicable. This manuscript does not contain any individual person's data in any form.

Availability of Data and Materials

The datasets generated and/or analyzed during the current study are available from the corresponding author upon reasonable request.

Competing Interests

The authors declare that they have no competing interests and have adhered to scientific ethics.

Authors' Information

- **Mustafa Sadeghi**: Master's student in Artificial Intelligence at Ferdowsi University of Mashhad
- **Mohamad Mehdi Khorsand Aalam**: Master's student in Artificial Intelligence at Ferdowsi University of Mashhad
- **Hadi Sadoghi Yazdi**: Full Professor, Department of Computer Engineering, Ferdowsi University of Mashhad, and affiliated with the Center of Excellence in Soft Computing and Intelligent Information Processing.